coatings

MDPI

Article

Lanthanum-Silica Sol-Gel Coatings for Protecting Metallic Materials in Museums: Approaches to Copper, Bronze, Lead and Steel

Javier Peña-Poza [1], Fernando Agua [1], Cristina Gil [2], María-Ángeles Villegas [1,*] and Manuel García-Heras [1]

[1] Instituto de Historia, CSIC, 28037 Madrid, Spain; javier.pena@cchs.csic.es (J.P.-P.); fernando.agua@cchs.csic.es (F.A.); manuel.gheras@cchs.csic.es (M.G.-H.)
[2] Facultad de Educación, Campus María Zambrano, Universidad de Valladolid, 40005 Segovia, Spain; cgil@dce.uva.es
* Correspondence: mariangeles.villegas@cchs.csic.es; Tel.: +34-916-022-672

Received: 9 February 2018; Accepted: 10 April 2018; Published: 12 April 2018

Abstract: Museum objects made from metals face the challenge of delaying corrosion in exhibition rooms, showcases and holdings. This study examined some innovative solutions used to protect such items based on sol-gel coatings doped with lanthanum. These coatings were prepared from sols based on TEOS as a precursor. Lanthanum acetate/nitrate was added as a doping agent and corrosion inhibitor. The coatings were deposited upon slabs of copper, bronze, lead and steel, since they are among the most common metals present in museums items. The coatings application was accomplished by immersion-extraction, and the remaining sols were gelled and characterized by Fourier transformed infrared spectroscopy and differential thermal analysis and thermogravimetry. To evaluate the behaviour and resistance of the coatings, tests of accelerated aging were carried out in climatic and Kesternich chambers, as well as under an atmosphere saturated with organic acids and under UV irradiation. The simulated conditions tested were undertaken to approach real conditions inside a conventional museum showcase. The microstructure of the coatings before and after accelerated aging tests was observed through optical and field emission scanning electron microscopies. The results indicated that these coatings can be a useful preventive, conservation avenue to protect copper, bronze and lead items exhibited in museums.

Keywords: metals; sol-gel coatings; protection; museum; accelerated ageing; corrosion

1. Introduction

Many museum objects and collections are composed of metals and alloys or, at least, have metallic components. As is known, the conservation of metals is critical to guard against the threat of corrosion, degradation and loss of material from the objects [1]. Since the thermodynamic trend of metal corrosion cannot be avoided, strategies to delay it as far as possible must be enhanced and investigated. Protection procedures, patination techniques and paint systems commonly used for modern metals and metallic objects cannot be applied with any guarantee of safety to historical materials and museum items [2,3]. This is because such items need nonaggressive products, easy application and reversibility as far as possible. Moreover, low-cost protective materials are preferred since museums budgets are limited.

Bearing this in mind, few conventional protective procedures are useful for metallic museum items. Among them, sol-gel coatings technology offers a suitable solution [4,5], even though the coatings' reversibility is only partial. Even so, it is a practical, versatile and inexpensive procedure

that can give more advantages than inconveniences for deeply corroded pieces and objects, e.g., archaeological items both unearthed and rescued from the sea waters.

Much research has been carried out on sol-gel formulations applied as consolidants for Heritage materials, e.g., different kinds of stones, Portland cement mortars, ceramic tiles, stained glasses, etc. In stones, sol-gel preparations were developed with the aim of reducing cracks inside the stone and/or to modify its hydrophobic character or porous size distribution [6–9]. The results seem to be promising, although some improvements are still needed. For instance, the simple TEOS gel compares less favorably with hydroxyapatite, which when formed at the grains boundaries, improves mechanical properties and yields low variations in porosity and pore size distribution. Moreover, some applications need the simultaneous use of a surfactant to achieve coarse and more uniform pore size to avoid cracks inside the stone [8,10]. For potash-lime-silicate glasses from medieval stained-glass windows, protective coatings based on sol-gel technology have proven to be good enough to guarantee adhesion and resistance against ageing and acids such as HCl, HNO_3 and H_2SO_4, even when applied without a thermal densification treatment [11,12]. However, silicon alkoxide/alkylalkoxide hybrid-based gels deposited upon ceramic tiles did not improve the protection provided by Paraloid B-72 (only one coat), even though some polymerization took place and the hydrophobic properties were partially modified by the sol-gel layer [13].

Concerning the usefulness of sol-gel coatings on metallic substrates, they have been widely proved upon steel, aluminum, zinc, magnesium, copper and their alloys [14–16], with the aim of replacing nonenvironmentally friendly Cr^{6+} anticorrosive compounds and improving the properties of the metallic substrate. Some strategies have been implemented: hybrid organic-inorganic formulations, multilayered coats, functional purposes, barrier effect, self-repairing mechanism, etc. Sol-gel protective coatings, upon the above-mentioned metals and alloys, also improve upon many industrial applications since these layers are resistant against water, oxidation, abrasion, etc. [17].

Sol-gel coatings doped with lanthanide compounds have been developed and applied for corrosion protection in a wide variety of metallic substrates and alloys [18–22]. These lanthanide compounds improve the sol-gel's protective benefits [23,24]. Moreover, some investigations have pointed out the capabilities of the combination of lanthanum salts and organic additives, such as benzotriazole and citric acid [25,26].

Corrosion protection measures for metallic museum items have been tested on objects exhibited in both showcases and in exhibition rooms, but these should also be carried out for items conserved in holdings and being transported, e.g., for temporary exhibitions. Therefore, the objectives of the present study were fitted as far as possible to deal with these issues. They can be summarized in three stages:

- Design of environmentally friendly sol-gel coatings doped with corrosion inhibitors: lanthanum salts.
- Production of these doped sol-gel coatings as a chemically active layer upon copper, bronze, lead and steel substrates.
- Study of the coatings' behaviour under laboratory conditions: thermal, structural, chemical and optical.

Two lanthanum salts have been investigated as corrosion inhibitors: lanthanum acetate and lanthanum nitrate. The former is believed to be a compatible compound both with the silica matrix to be formed by hydrolysis and partial polycondensation of silicon tetraethoxide, and with the solvent to be used during the sol preparation (ethanol). The $–CH_2–CH_3$ group is present in these three sol components (silica matrix precursor, solvent and dopant), which could improve the gel's homogeneity in terms of residual organic matter entrapped in the silica network. Moreover, the acetate ions will remain in the gel stage since their thermal decomposition is expected to be at about 450–480 °C (lanthanum oxycarbonate formation) and above 910 °C (lanthanum oxide formation) [27,28]. The latter, lanthanum nitrate, was chosen for its lower release temperature of NO_3^- groups (from ~60 °C) with

respect to that of $–CH_2–CH_3$ groups (~450 °C), which could favour the partial thermal densification of the doped coatings.

2. Materials and Methods

The metal substrates used were copper, bronze, lead and steel slabs from 1.0 to 1.5 mm in thickness and at about 20 mm × 30 mm in size. These metallic substrates were selected on the basis of their frequent presence in cultural heritage items, particularly in museums environments. Tables 1–4 show, respectively, the results of the chemical analyses carried out for these metallic substrates. Such analyses were undertaken by the respective suppliers.

Table 1. Chemical composition of the copper substrates.

Substrates	Chemical Composition (wt %)	
Copper	Cu 99.95	Others rest

Table 2. Chemical composition of the bronze substrates.

Substrates	Chemical Composition (wt %) (min–max)					
Bronze	Cu rest	Sn 6–8	Pb 5–8	Zn 3.5–5.5	Ni 0–2	Others 0–1

Table 3. Chemical composition of the lead substrates.

Substrates	Chemical Composition (wt %)									
Lead	Cu 0.0319	Sn 0.0004	Zn 0.0003	Fe 0.0007	Sb 0.0005	Bi 0.0233	As 0.0002	Ag 0.0016	Cd 0.0009	Pb rest

Table 4. Chemical composition of the steel substrates.

Substrates	Chemical Composition (wt %)						
Steel	Fe rest	C 0.052	Mn 0.246	P 0.019	S 0.024	Si 0.007	Al 0.051

The sol-gel coatings matrix was obtained from tetraethoxysilane (TEOS) and the active sol-gel dopants were lanthanum acetate and lanthanum nitrate, used separately. Other sol components were absolute ethanol, HNO_3 0.01–0.10 M (up to pH ~3 in the corresponding sols) and distilled water. All the chemicals used were analytical grade reagents. The scheme of Figure 1 summarizes the synthesis steps.

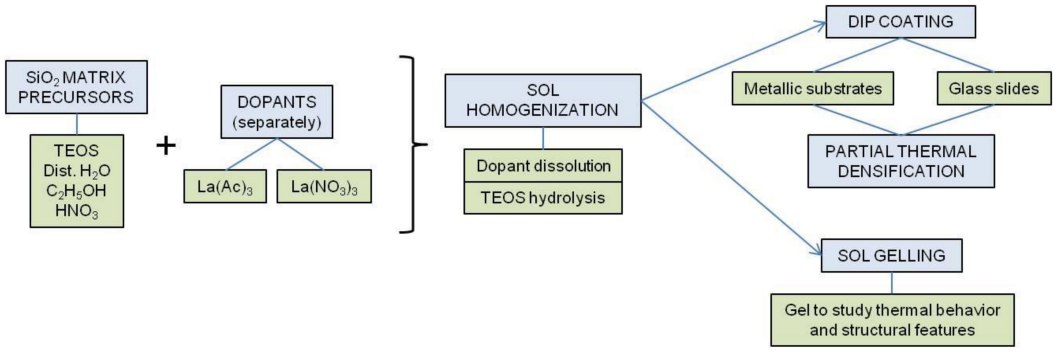

Figure 1. Scheme of the synthesis steps for obtaining sol-gel coatings and bulk gels.

The sol-gel formulation was calculated to obtain a theoretical mol composition of $1La_2O_3 \cdot 99SiO_2$ (theoretical total densification of the corresponding gel). The sol silica matrix consisted of 1 mol TEOS, 3 mol distilled water, 8 mol absolute ethanol and the necessary volume of HNO_3 to get a sol pH ~ 3. The mixture, once stirred and homogenized, yields a pre-hydrolyzed silica sol to which the active La^{3+}-dopant was added (0.02 mol $La(CH_3COO)_3$, ($La(Ac)_3$) or 0.02 mol $La(NO_3)_3$). After dissolution of the lanthanum salt and further homogenization of the sols, they were ready to be applied as coatings upon the metallic substrates. For comparison purposes, a pure-silica-undoped sol was also prepared to coat the substrates.

The coatings deposition was carried out by dipping, using a home-made device at a constant withdrawal rate of 2 mm s^{-1}, under controlled environmental conditions (25 °C and 35% relative humidity). The partial thermal densification of the coatings was accomplished in a forced air stove at 60 °C for 72 h. Under such conditions the average coatings' thickness was about 220 ± 15 nm, as estimated by the interference fringe method from the corresponding UV-Vis transmittance spectra of the coated samples [29].

Apart from the coated metallic samples, common glass slides were additionally coated with the same sols to be used in the optical coatings characterization since, for this purpose, transparent and colourless substrates are needed. Moreover, the remaining sols, once all the coatings were applied, were gelled in a forced air stove at 35 °C for 48 h, and then grounded to a fine powder to be used for the structural and thermal characterization of the gels used to obtain the coatings.

The macroscopic aspect of the coatings both on metallic and glass substrates was homogeneous, transparent and colourless.

The UV-Vis transmittance spectra of the coated glass samples were recorded with a Shimadzu 3100 double-beam spectrophotometer (Shimadzu Corporation, Kyoto, Japan) equipped with an integrating sphere. Samples were placed behind a 1 mm width slit mask and the spectra were recorded from 200 to 800 nm with 0.5 nm spectral resolution.

The thermal behaviour of the coatings (grounded gelled materials) was analyzed by differential thermal analysis (DTA) and thermogravimetric analysis (TGA) using a TA Instruments equipment model Q-600 (Waters Corporation, Milford, MA, USA), with a platinum sample holder under air atmosphere and a heating rate of 10 °C min^{-1} up to 700 °C.

The structural features of the coatings (grounded gelled materials) were investigated by Fourier transformed infrared (FTIR) spectroscopy. The spectra were recorded on the powdered samples diluted in anhydrous KBr (pellets technique) with a spectrometer Perkin Elmer model Spectrum BX (Perkin Elmer Inc., Waltham, MA, USA).

The quality of the coatings was checked with conventional optical microscopy (OM), and petrographic microscopy (PM) observations. The optical microscope was a Motic 168 (Motic Microscopy, Hong Kong, China), and the petrographic one was a Kyowa Bio-Pol 2 polarizing light microscope (Kyowa Electronic Instruments Co. Ltd., Tokyo, Japan). Micrographs were recorded with a Moticam 2500 digital camera.

The chemical resistance of the coatings was tested by accelerated ageing cycles in a climatic chamber Dycometal model CCK-81 following the ISO-9142 standard [30], and in a Kesternich chamber Dycometal model VCK-300 under SO_2 atmosphere following the DIN-50018 standard [31]. Additionally, some other resistance tests were carried out: (i) under an organic acids atmosphere (mixture of HCOOH and CH_3COOH, since these are the chemicals usually present in the emissions inside museum showcases [32]); and (ii) optical-ultraviolet (UV) irradiation tests carried out for 21 days, at least. Table 5 summarizes the experimental details of the weathering, chemical and optical resistance tests carried out.

The microstructural and textural features of the coatings were observed by field emission scanning electron microscopy (FESEM) with a Hitachi S4800FEM equipment (Hitachi, Tokyo, Japan). Local chemical analyses were undertaken by energy dispersive X-ray spectrometry (EDS) with an Oxford X-Max EDS micro-analyzer attached to the microscope.

Table 5. Experimental details of the weathering and chemical treatments carried out.

Treatment	Test Equipment	Conditions	Time
Accelerated ageing	Climatic chamber	Standard ISO-9142 23 °C 85% RH 1 day 55 °C 28% RH 1 day 23 °C 85% RH 3 days 55 °C 28% RH 2 days	21 days
Accelerated ageing under SO_2 atmosphere	Kesternich corrosion chamber	Standard DIN 50018 40 °C 100% RH 0.5 L SO_2 8 h closed door 16 h open door	1 cycle
Organic acids	Desiccator	Acetic acid + formic acid (0.01 vol. %) saturated atmosphere	7 days
UV irradiation	UV lamp	300 W	21 days

3. Results

3.1. Thermal Behaviour

Figure 2 shows the DTA-TGA diagrams for the undoped pure-silica gel as well as for the gels doped with lanthanum acetate and lanthanum nitrate.

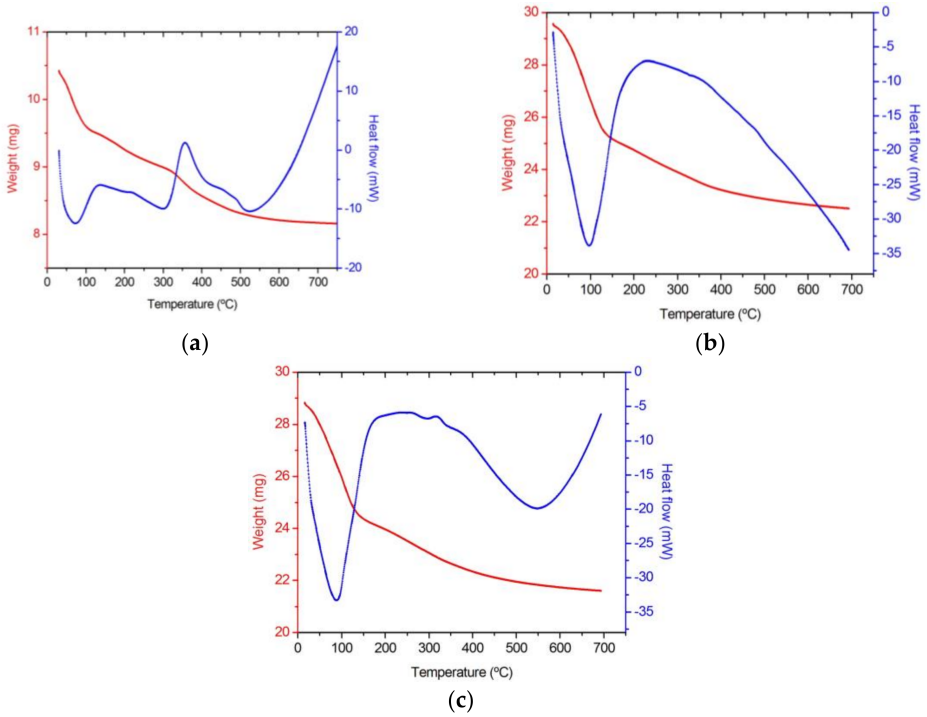

Figure 2. DTA and TGA diagrams of some of the samples studied. (**a**) Pure SiO_2 gel; (**b**) $La(Ac)_3$ doped gel; (**c**) $La(NO_3)_3$ doped gel.

Table 6 summarizes the assignments of the thermal effects detected and the corresponding weight losses for the same gel samples. The thermal effects in lanthanum-doped gels are similar to those of the pure-silica-undoped gel, but some of them overlap. In addition, the incorporation of both lanthanum dopants delays the loss of adsorbed water and alcohols from the sol and the oxidation of the organic precursors. Therefore, a progressive delay of the thermal evolution of the sol-gel matrix takes place.

Table 6. DTA and TGA assignments of some of the samples studied.

Gel Sample	DTA		TGA	
	T (°C)	Effect	*T* (°C)	Effect
100 SiO_2 Blank	73	ENDO Loss adsorbed water and alcohols	Room-100	Great loss of water and alcohols
	130–220	EXO Organic precursors oxidation	100–300	Great loss due to organic matter release
	356	EXO Organic groups decomposition	300–400	
	522	ENDO Si-OH groups release	500–600	Small loss of chemically bonded water
$1La_2O_3 \cdot 99SiO_2$ $La(Ac)_3$	97	ENDO Loss adsorbed water and alcohols	Room-135	Great loss of water and alcohols
	130–275	EXO Organic precursors oxidation	130–400	Great loss due to organic matter release
	350	EXO Organic groups decomposition		
	500–	ENDO Si-OH groups release	500–	Progressive loss of chemically bonded water
$1La_2O_3 \cdot 99SiO_2$ $La(NO_3)_3$	87	ENDO Loss adsorbed water and alcohols	Room-140	Great loss of water and alcohols
	140–295	EXO Organic precursors oxidation	140–400	Great loss due to organic matter release
	300–400	EXO Organic groups decomposition		
	545	ENDO Si-OH groups release	500–	Progressive loss of chemically bonded water

TGA diagrams give some additional information on the gels' behavior (Table 7). At the temperature of partial densification of the coatings (60 °C), the smallest weight loss percentage corresponds to the undoped sample, while in the doped samples it is slightly higher due to the release of adsorbed water additionally associated with the lanthanum salts and perhaps ethanol. The highest weight loss percentage of the $La(NO_3)_3$ doped sample could be explained by the early decomposition of nitrate groups at about 60 °C, which cannot be discarded. Regarding the temperatures at which the 5% weight loss takes place, they decrease from the undoped sample to the doped ones, and the sample doped with $La(NO_3)_3$ shows the lowest value for the same reason stated above: the beginning of the nitrates' decomposition. Likewise, the final weight loss percentages at the end of the test (~700 °C) increase from the undoped sample to the $La(Ac)_3$ and to the $La(NO_3)_3$ doped samples, which indicates some more intense densification of doped samples. Temperatures and weight loss percentages at which the maximum weight loss rates occur in each sample indicate that both doped samples behave similarly, while the undoped sample losses the lowest weight at the lowest temperature. This could be explained by the early release of water and ethanol in the pure silica sol-gel network not disturbed by dopants.

Table 7. Additional data concerning TGAs of some of the samples studied.

Dopant in the Coating	Weight Loss at 60 °C (%)	Temperature at Which 5% Weight Loss Occurs (°C)	Final Weight Loss at 700 °C (%)	Temperature at Which Maximum Weight Loss Rate Occurs (°C)	Weight Loss at the Maximum Weight Loss Rate (%)
None (blank)	3.36	71.67	21.59	65.17	4.03
$La(Ac)_3$	3.55	70.26	23.88	94.91	9.03
$La(NO_3)_3$	4.06	67.10	25.05	89.94	8.47

3.2. Structural Features

FTIR spectra of doped and undoped gel samples are shown in Figure 3. The main vibration assignments are summarized in Table 8.

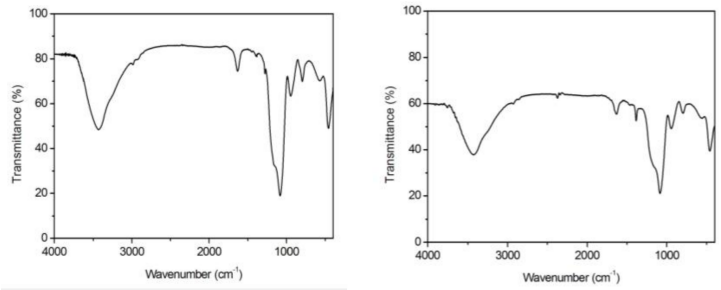

(**a**) (**b**)

Figure 3. *Cont.*

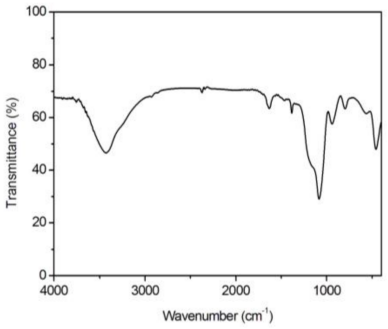

(**c**)

Figure 3. FTIR spectra of some of the samples studied. (**a**) Pure SiO_2 gel; (**b**) $La(Ac)_3$ doped gel; (**c**) $La(NO_3)_3$ doped gel.

The bands and assignments of the pure-silica-undoped sample are also present or shifted in the lanthanum-acetate-doped sample, which in addition shows other bands due to $La(Ac)_3$. The same occurs for the lanthanum-nitrate-doped sample, which in addition shows other bands due to $La(NO_3)_3$. However, no bands due to chemical bonds such as La–O–Si were identified [33–35]. This means that La^{3+}-ions are physically entrapped in the pores of the silica sol-gel network and, hence, they remain free enough to react during a common corrosion process.

Table 8. FTIR assignments of some of the samples studied [36–38].

Gel Sample	Wavenumber (cm^{-1})	Assignment	Intensity [1]	Observations
100 SiO_2 Blank	465	δ Si–O–Si	XXXX	Siloxane matrix
	577; 801	ν*s* Si–O–Si	XXX; XXX	Siloxane matrix
	951	ν Si–OH	XXX	Raw alkoxides
	1085	ν Si–O; ν*as* Si–O	XXXXX	$Si–OCH_3$; Si–O–Si
	1166	ν*s* C–O	XXXXX, x	Raw alkoxides
	1286	ν*as* C–O	XX, x	Raw alkoxides
	1398; 1450	δ CH_2	X; X	Si–R
	1637	ν C=C	XXX	Raw alkoxides
	2921; 2988	ν C–H; ν C–H	X; X	Si–R; $–OCH_2CH_3$
	3430	ν O–H	XXXXX	Si–OH
$1La_2O_3·99SiO_2$ $La(Ac)_3$	463	δ Si–O–Si ; π COO–	XXX	Siloxane matrix; $La(Ac)_3$
	564	ν La–O	XXX	$La(Ac)_3$
	800	ν*s* Si–O–Si	XXX	Siloxane matrix
	948	ν Si–OH; ν C–C	XXX	Raw alkoxides; $La(Ac)_3$
	1083	ν Si–O; ν*as* Si–O; ν CH_3	XXXXX	$Si–OCH_3$; Si–O–Si; $La(Ac)_3$
	1154	ν*s* C–O	XXXXX, x	Raw alkoxides
	1384	δ*s* CH_3	XXX	$La(Ac)_3$
	1460	δ*as* CH_3	X	$La(Ac)_3$
	1632	ν C=C	XXX	Raw alkoxides
	2854; 2925	ν*s* C–H; ν C–H	X	$La(Ac)_3$; Si–R
	3433	ν O–H	XXXXX	Si–OH
$1La_2O_3·99SiO_2$ $La(NO_3)_3$	457	δ Si–O–Si	XXXX	Siloxane matrix
	565	ν La–O	XXX	$LaO(NO_3)$
	798	ν NO_3^-	XXX	$La(NO_3)_3$
	944	ν Si–OH	XXX	Raw alkoxides
	1084	ν Si–O; ν*as* Si–O	XXXXX	$Si–OCH_3$; Si–O–Si
	1160	ν*s* C–O	XXXXX, x	Raw alkoxides
	1387; 1463	δ CH_2	X; X	Si–R
	1632	ν C=C	XXX	Raw alkoxides
	2850; 2925	ν*s* C–H	X	Si–R
	3429	ν O–H	XXXXX	Si–OH

Note: [1] XXXXX very intense; XXXX intense; XXX medium; XX low; X very low; x shoulder.

3.3. Macroscopic Quality

After the accelerated ageing treatment in the climatic chamber, all the metallic coated substrates resist well the weathering conditions (up to 55 °C and 85% relative humidity, 21 days). After the treatment in the Kesternich chamber, which simulates a polluted environment (up to 40 °C and 100% relative humidity under SO_2 atmosphere), copper, bronze and lead coated samples do not show deterioration or corrosion signs, while small surface pits appeared in coated steel. The same occurs after treatment under a mixture of organic acids (formic and acetic acids), i.e., only the coated steel samples show deterioration signs and the formation of more or less interconnected pits (Figure 4).

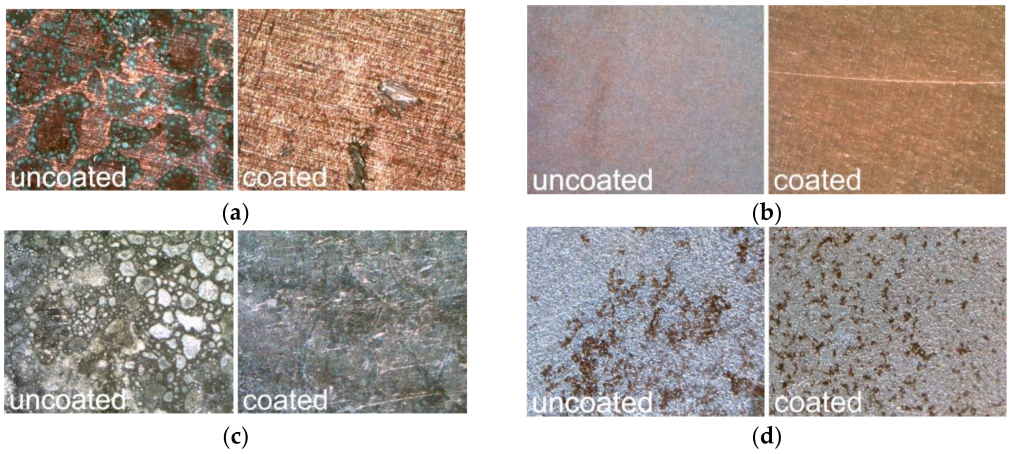

Figure 4. MO images of uncoated and coated areas of some of the samples studied after the weathering tests indicated. (**a**) Copper, x14, $La(NO_3)_3$ doped coating, Kesternich Chamber; (**b**) Bronze, x14, $La(Ac)_3$ doped coating, organic acids treatment; (**c**) Lead, x14, $La(NO_3)_3$ doped coating, Kesternich Chamber; (**d**) Steel, x7, $La(NO_3)_3$ doped coating, organic acids treatment.

PM observations pointed out both the optical quality and the resistance of coatings after the accelerated weathering tests were carried out. For instance, Figure 5 shows the aspect of one of the glass slides coated with $La(Ac)_3$ doped silica after the most aggressive treatment under the Kesternich chamber conditions. Apart from the typical conchoidal fractures due to the glass piece cutting, no signs of alteration can be identified in the PM image, as well as in the corresponding OM image.

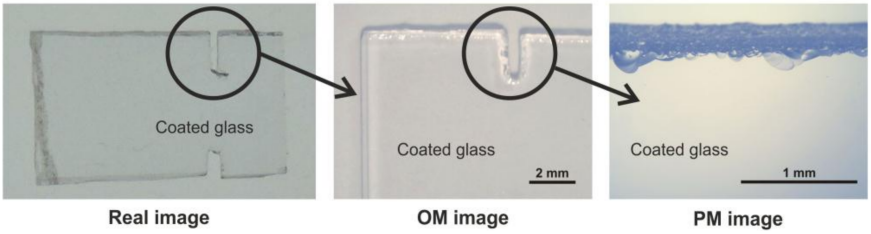

Figure 5. Photograph, OM image and PM image of a glass slide piece coated with $La(Ac)_3$ doped silica after the treatment in the Kesternich chamber.

All the coated samples were irradiated with UV light for at least 21 days, and after this treatment the coatings' appearance upon metallic substrates is neutral, colorless and transparent, with the same aspect as before the irradiation, except for the steel substrates in which the coated area appeared slightly yellowish. Nevertheless, no deterioration signs were observed in any kind of samples.

Concerning the optical quality of the coated samples, Vis transmission spectra recorded on glass slides coated with lanthanum-doped silica (Figure 6) show transmission percentages slightly higher than on the uncoated glass slide. This is attributed to the higher refractive index of the uncoated glass

slide related to the lanthanum-doped silica coatings. Therefore, the optical quality of lanthanum-doped coatings is optimal to preserve the original appearance of metallic substrates in terms of brightness and reflection.

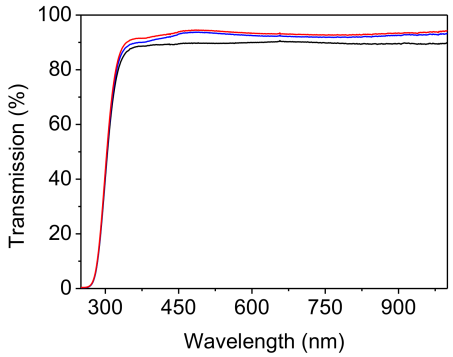

Figure 6. Visible spectra of some of the samples studied. Black line: uncoated common glass slide. Blue line: glass slide coated with $La(Ac)_3$ doped silica. Red line: glass slide coated with $La(NO_3)_3$ doped silica.

3.4. Microstructural Features

A selection of micrographs corresponding to the results after the most aggressive treatments are shown in this section for each kind of metallic substrate, even though all possible combinations of accelerated weathering tests and metallic substrates coated with the two lanthanum active dopants were carried out and observed by FESEM.

In copper substrates after the treatment in the Kesternich chamber (Figure 7a), the uncoated area shows a heterogeneous surface of corrosion crust with quickly crystallized precipitates (Figure 7b), while in the coated area the sol-gel layer doped with $La(NO_3)_3$ appears cracked and a precipitate emerging from the metallic substrate is slowly formed near the cracks (Figure 7c).

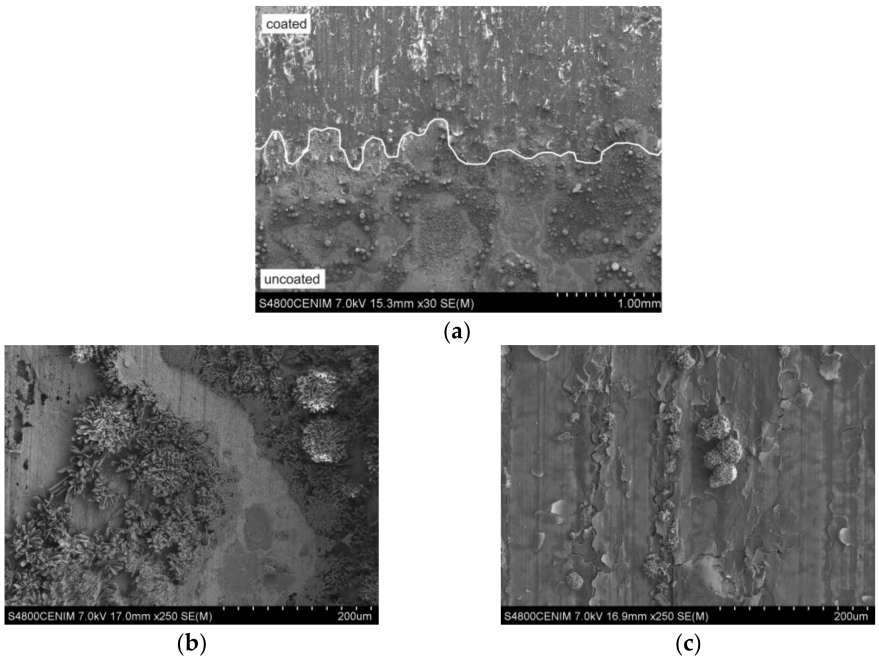

Figure 7. (**a**) FESEM image of a copper substrate in the coated/uncoated interface ($La(NO_3)_3$ doped coating) after the weathering test in the Kesternich Chamber; (**b**) Detail of the uncoated area; (**c**) Detail of the coated area.

Figure 8a shows a FESEM micrograph of a bronze substrate after treatment under organic acids atmosphere. A corrosion crust with abundant precipitates is formed in the uncoated area (Figure 8b). However, the sol-gel layer doped with $La(Ac)_3$ is preserved in the coated area in which the first signs of a precipitate formation can be observed (Figure 8c).

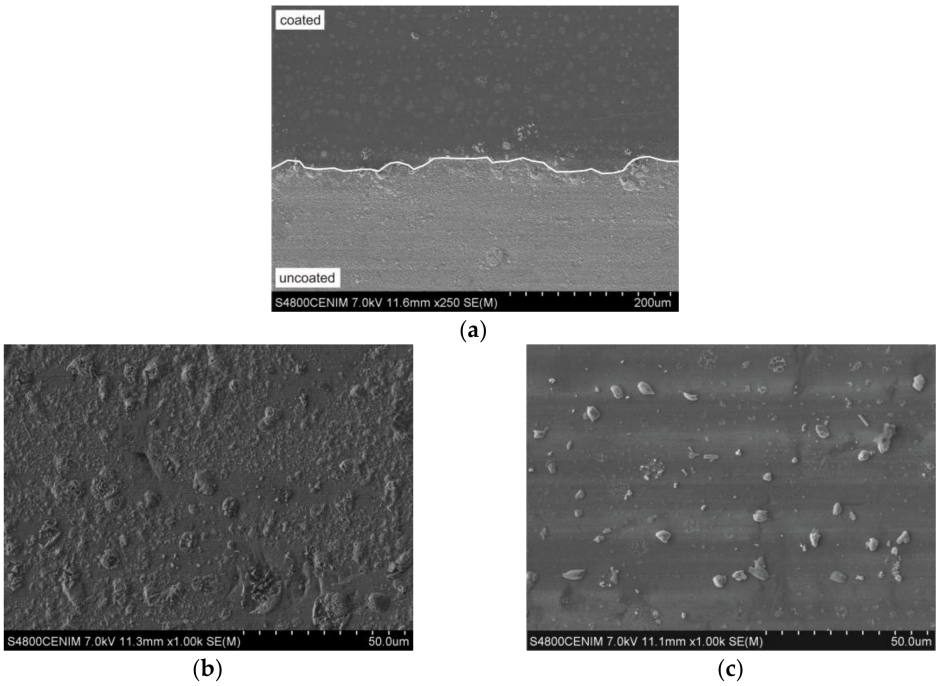

Figure 8. (**a**) FESEM image of a bronze substrate in the coated/uncoated interface ($La(Ac)_3$ doped coating) after the weathering test under organic acids atmosphere; (**b**) Detail of the uncoated area; (**c**) Detail of the coated area.

After the organic acids treatment, the lead substrates (Figure 9a) in the uncoated area show a corrosion crust formed by heterogeneous precipitates (Figure 9b). In the corresponding coated area, the sol-gel layer, doped with $La(Ac)_3$, is preserved and a very homogeneous precipitate appears (Figure 9c).

FESEM observations carried out in steel substrates after treatment in the climatic chamber present noticeable differences between the microstructure of coated and uncoated areas. Similar to the former cases, the uncoated area shows a corrosion crust composed of quickly crystallized heterogeneous precipitates (Figure 10a). In the coated area, the coating was deposited upon the lower steel surface (polishing valleys) and the first signs of precipitation upon the higher steel surface can be observed (Figure 10b).

The results obtained after the treatment in the Kesternich chamber revealed that the sol-gel coating fails and a thick corrosion crust was formed. The results were even worse after treatment under organic acids atmosphere: in both doped $La(Ac)_3$ and $La(NO_3)_3$ coatings, the sol-gel coating was cracked on the coated area and precipitates appear from the metallic bulk of the sample (Figure 11a,b, respectively).

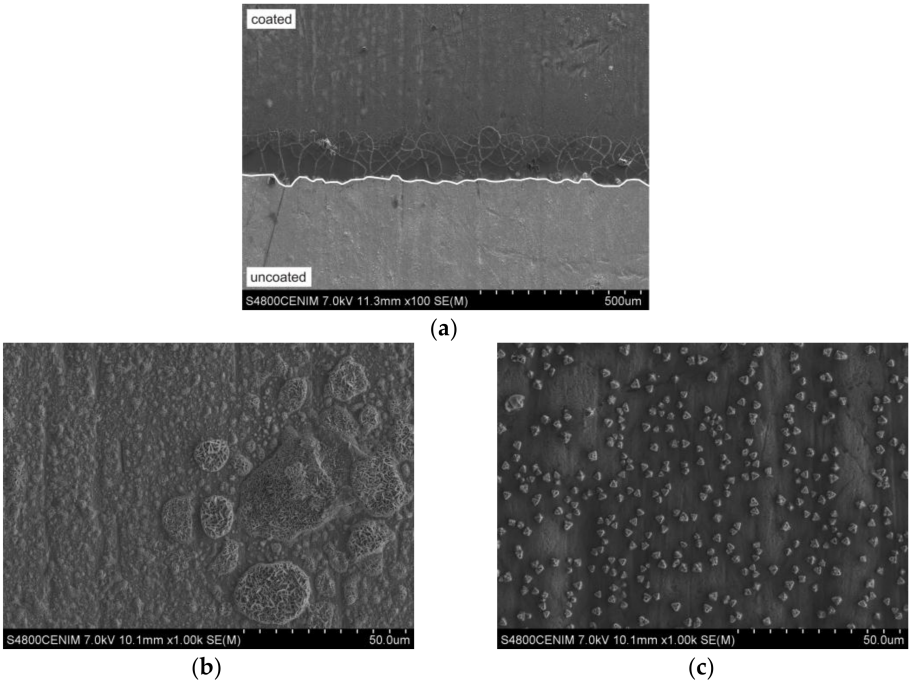

(**a**) (**b**) (**c**)

Figure 9. (**a**) FESEM image of a lead substrate in the coated/uncoated interface ($La(Ac)_3$ doped coating) after the weathering test under organic acids atmosphere; (**b**) Detail of the uncoated area; (**c**) Detail of the coated area.

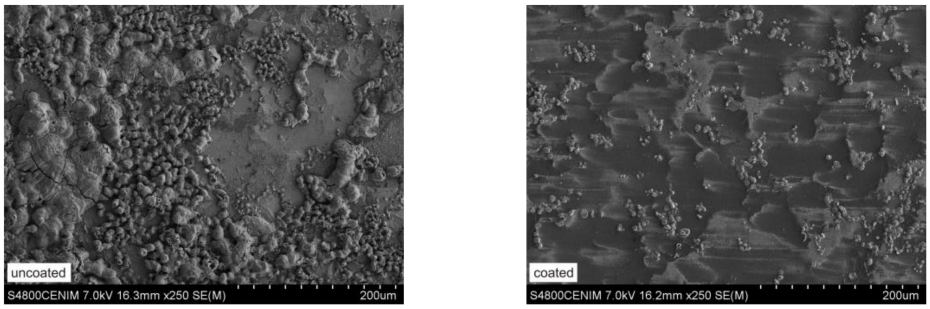

(**a**) (**b**)

Figure 10. FESEM image of a steel substrate after the weathering test in the climatic chamber: (**a**) Uncoated area; (**b**) Coated area ($La(Ac)_3$ doped coating).

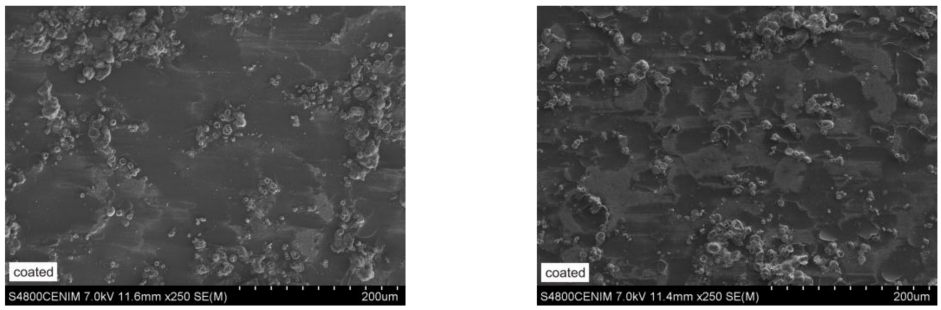

(**a**) (**b**)

Figure 11. FESEM image of a steel substrate after the weathering test under organic acids atmosphere: (**a**) Coated area ($La(Ac)_3$ doped coating); (**b**) Coated area ($La(NO_3)_3$ doped coating).

In this case, the sol-gel coating is cracked and also covers the lower steel surface, while the upper steel surface remains almost uncoated. This is due to the low thickness of the sol-gel layer applied (at about 220 nm). Therefore, a thicker layer would be needed to cover both lower and upper surfaces of the steel substrate.

4. Discussion

As is known, sol-gel silica matrices are partially porous materials even when deposited as thin coatings, as they were prepared here (~220 nm). Such residual porosity is preserved when the thermal densification is carried out at a moderate temperature (60 °C in the present work), and this enhances the reactivity of the sol-gel components, including the active dopants (La^{3+}-ions). In this sense, DTA-TGA results pointed out the additional improvement provided by the incorporation of La^{3+}-ions into the sol-gel silica network, since a progressive delay of the thermal evolution of the sol-gel matrix occurs, which extends the range of the thermal activity of dopants to face the corrosive processes to be produced and then mitigated.

Moreover, La^{3+}-ions are not chemically bonded to the sol-gel silica network, as is demonstrated by the FTIR spectra recorded. This means that they are probably physically entrapped in the porous network and, hence, they are able to react both with external chemicals (e.g., pollutant emissions) and with the metallic substrates. In other words, they are free to behave as an active (reactive) corrosion inhibitor.

As the OM and PM observations and Vis spectrometry demonstrated at the macroscopic scale, the lanthanum-doped coatings provide all physical properties desired, i.e., adequate transparency, achromacity and optimal optical transmission. Thus, they will not change at all the original aspects of the metallic substrates in terms of brightness and reflection. This is an important subject for objects of cultural heritage interest, e.g., museum items, valuable and historical pieces and objects.

The coated (both lanthanum acetate and nitrate) copper substrates resist well the chemical attack of the accelerated treatments carried out in the climatic chamber, under organic acids atmosphere and with UV irradiation. Since the coating remains unaltered, it works as a barrier layer in these cases. However, when coated copper substrates are exposed to an artificial polluted environment (in the Kesternich chamber under SO_2 atmosphere), coating breakage occurs and the beginning of a slow precipitation is observed (Figure 7). The emerging precipitate is deposited in the microcracks and seals the surface. Thus, a self-repairing mechanism takes place.

Coated (both lanthanum acetate and nitrate) bronze substrates are resistant to all the treatments tested. Nevertheless, the samples treated under the organic acids atmosphere showed some initial signs of surface precipitation, even though the coating is preserved (no cracks appeared) (Figure 8). This means that in bronze substrates the sol-gel coatings have provided a protective barrier effect.

A similar behavior against the accelerated weathering treatments was observed in coated lead substrates. In these samples the sol-gel coating is preserved and a very homogeneous precipitate appears upon the surface (Figure 9). Once again, a protective barrier effect takes place against corrosion.

Coated steel substrates (both doped with lanthanum acetate and nitrate) are resistant against the climatic chamber treatment and the UV irradiation (protective barrier effect). However, they show macroscopic corrosion signs after the treatments carried out in the Kesternich chamber and under the organic acids atmosphere: the sol-gel coating remains deposited on the lower steel surface due to residual polishing roughness, while the upper surface parts were almost uncoated. This is due to the very low thickness of the sol-gel coating (~220 nm). As a consequence the coating fails and a corrosion crust is formed on the surface (Figure 10). Moreover, in some cases (e.g., lanthanum-nitrate-doped coating after the organic acids treatment) the coating appeared cracked with disperse heterogeneous precipitate not accumulated in the cracks. Thus, neither the protective barrier effect nor the self-repairing mechanism took place.

Taken into account the former issues, the proposed mechanism is as follows. The initial state of the coated metallic substrates exposed to a regular environment (air) is characterized by the presence of

Si–O–Si siloxane network, Si–OH terminal silanol groups, La^{3+}-ions in interstitial sites and/or solvated in open pores of the silica matrix. Further, during the accelerated weathering and chemical resistance tests the oxygen reduction

$$½\ O_2 + H_2O + 2\ e^- \rightarrow 2\ OH^- \quad (1)$$

takes place as the cathodic reaction, and the metal oxidation occurs

$$Me^0 \rightarrow Me^{n+} + n\ e^- \quad (2)$$

as the anodic reaction. In this situation, La^{3+}-ions can react and behave as a corrosion inhibitor following, for instance, some precipitation or complexation

$$La^{3+} + 3\ OH^- \rightarrow La(OH)_3\downarrow \quad (3)$$

The products of such reactions would be the chemical species responsible for the self-repairing mechanism when homogeneous, fine-grain sized particles (precipitate) are deposited near the micro-cracks and thereby sealing them.

5. Conclusions

Concentration of 1 mol % La_2O_3 with respect to the sol-gel coating formulation has proven to be adequate for La^{3+}-ions to remain entrapped in interstitial sites of the silica matrix, thereby behaving as an active corrosion inhibitor.

The anticorrosive behavior of La^{3+}-ions proceeds by means of a self-repairing mechanism, probably by precipitation of lanthanum oxo-hydroxydes and/or formation of coordination complexes.

Weathering and chemical resistance of lanthanum-doped coatings upon the metallic substrates tested is good enough to ensure a protective role of these sol-gel coatings upon copper, bronze and lead, while steel substrates need thicker coatings.

Acknowledgments: J. Rubio, Ceramic and Glass Institute (CSIC) for thermal analysis and infrared spectra. Project MINEICO/FEDER MAT2015-65445-C2-2-R and program Geomateriales 2 ref. S2013/MIT-2914 (CAM-EU) for financial support. TechnoHeritage Network on Science and Technology for the Conservation of Cultural Heritage for professional support.

Author Contributions: M.-A.V. has been the principal investigator and she has written the manuscript with the collaboration of C.G. and M.G.-H. J.P.-P. and F.A. have carried out the experiments and elaborated the manuscript images. The scientific discussion of results and their interpretation has been done by J.P.-P., F.A., C.G., M.-A.V. and M.G.-H. All the authors have read and approved the final version of the manuscript

Conflicts of Interest: The authors declare no conflict of interest.

References

1. Chico, B.; de la Fuente, D.; Morcillo, M. Corrosión atmosférica de metales en condiciones climáticas extremas. *Bol. Soc. Esp. Ceram. Vidr.* **2000**, *39*, 329–332. (In Spanish) [CrossRef]
2. Black, L.; Allen, G.C. Nature of lead patination. *Brit. Corros. J.* **1999**, *34*, 192–197. [CrossRef]
3. Julve, E. Un fenómeno corrosivo deseable: La atractiva pátina verde de los edificios nórdicos y centroeuropeos. *An. Quím.* **2006**, *102*, 68–72. (In Spanish)
4. Bethencourt, M.; Botana, F.J.; Calvino, J.J.; Marcos, M.; Rodríguez-Chacón, M.A. Lanthanide compounds as environmentally friendly corrosion inhibitors of aluminum alloys. A review. *Corros. Sci.* **1998**, *40*, 1803–1819. [CrossRef]
5. Dumont, B.; Thiery, R.; Welter, J.M.; Duterne, M. Hybrid sol-gel clear coatings for decoration brass profiles. *Rev. Met. Paris* **2001**, *98*, 783–788. [CrossRef]
6. Zárraga, R.; Cervantes, J.; Salazar-Hernández, C.; Wheeler, G. Effect of the addition of hydroxyl-terminated polydimethylsiloxane to TEOS-based stone consolidants. *J. Cult. Herit.* **2010**, *11*, 138–144. [CrossRef]
7. Barberana-Fernández, A.M.; Carmona-Quiroga, P.M.; Blanco-Varela, M.T. Interaction of TEOS with cementitious materials: Chemical and physical effects. *Cem. Concr. Compos.* **2015**, *55*, 145–152. [CrossRef]

8. Mosquera, M.J.; de los Santos, D.M.; Rivas, T. Surfactant-synthesized ormosils with application to stone restoration. *Langmuir* **2010**, *26*, 6737–6745. [CrossRef] [PubMed]
9. Franzoni, E.; Graziani, G.; Sassoni, E. TEOS-based treatments for stone consolidation: Acceleration of hydrolysis-condensation reactions by poulticing. *J. Sol Gel Sci. Technol.* **2015**, *74*, 398–405. [CrossRef]
10. Mosquera, M.J.; de los Santos, D.M.; Rivas, T.; Sanmartín, P.; Silva, B. New nanomaterials for protecting and consolidating stone. *J. Nano Res.* **2009**, *8*, 1–12. [CrossRef]
11. De Bardi, M.; Hutter, H.; Schreiner, M.; Bertoncello, R. Sol–gel silica coating for potash–lime–silica stained glass: Applicability and protective effect. *J. Non Cryst. Solids* **2014**, *390*, 45–50. [CrossRef]
12. Dal Bianco, B.; Bertoncello, R. Sol–gel silica coatings for the protection of cultural heritage glass. *Nucl. Instrum. Met. Phys. Res. B* **2008**, *266*, 2358–2362. [CrossRef]
13. Constâncio, C.; Franco, L.; Russo, S.; Ajinho, C.; Pires, J.; Vaz, M.F.; Carvalho, A.P. Studies on polymeric conservation treatments of ceramic tiles with Paraloid B-72 and two alkoxysilanes. *J. Appl. Polym. Sci.* **2010**, *116*, 2833–2839. [CrossRef]
14. Zucchi, F. Sol-gel coatings for the preservation of metallic heritage artefacts. In *Corrosion and Conservation of Cultural Heritage Metallic Artefacts*, 1st ed.; Dillmann, P., Watkinson, D., Angelini, E., Adriaens, A., Eds.; European Federation of Corrosion (EFC) Series; Woodhead Publishing Limited: Oxford, UK, 2013; pp. 540–551, ISBN 9781782421542.
15. Figueira, R.B.; Fontinha, I.R.; Silva, C.J.R.; Pereira, E.V. Hybrid sol-gel coatings: Smart and green materials for corrosion mitigation. *Coatings* **2016**, *6*, 12. [CrossRef]
16. Figueira, R.B.; Silva, C.J.R.; Pereira, E.V. Organic–inorganic hybrid sol–gel coatings for metal corrosion protection: A review of recent progress. *J. Coat. Technol. Res.* **2014**, *12*, 1–35. [CrossRef]
17. Wang, D.; Bierwagen, G.P. Sol–gel coatings on metals for corrosion protection. *Prog. Org. Coat.* **2009**, *64*, 327–338. [CrossRef]
18. Arenas, M.A.; Bethencourt, M.; Botana, F.J.; de Damborenea, J.; Marcos, M. Inhibition of 5083 aluminum alloy and galvanised steel by lanthanide salts. *Corros. Sci.* **2001**, *43*, 157–170. [CrossRef]
19. García-Heras, M.; Jiménez-Morales, A.; Casal, B.; Galván, J.C.; Radzki, S.; Villegas, M.A. Preparation and electrochemical study of cerium-silica sol-gel thin films. *J. Alloys Compd.* **2004**, *380*, 219–224. [CrossRef]
20. Montemor, M.F.; Ferreira, M.G.S. Corrosion performance of a two-step pre-treatment for galvanized steel based on lanthanum nitrate and silanes. *Surf. Interface Anal.* **2004**, *36*, 773–776. [CrossRef]
21. Xiaoxiao, W.; Gang, K.; Ziwen, S.; Chunshan, C. Preparation and corrosion performance of lanthanum nitrate conversion coating on hot-dip Galfan steel. *Chin. J. Mater. Res.* **2016**, *30*, 269–276. [CrossRef]
22. Yasakau, K.A.; Zheludkevich, M.L.; Ferreira, M.G.S. Lanthanide salts as corrosion inhibitors for AA5083. Mechanism and efficiency of corrosion inhibition. *J. Electrochem. Soc.* **2008**, *155*, C169–C177. [CrossRef]
23. Bethencourt, M.; Botana, F.J.; Cauqui, M.A.; Marcos, M.; Rodríguez, M.A.; Rodríguez-Izquierdo, J.M. Protection against corrosion in marine environments of AA5083 Al-Mg alloy by lanthanide chlorides. *J. Alloys Compd.* **1997**, *250*, 455–460. [CrossRef]
24. Abuín, M.; Serrano, A.; Llopis, J.; García, M.A.; Carmona, N. Silica doped with lanthanum sol–gel thin films for corrosion protection. *Thin Solid Films* **2012**, *520*, 5267–5271. [CrossRef]
25. Fan, H.; Li, S.; Shi, Z.; LV, X.; Zhao, Z. Studies of the conversion coatings formed by combined use of lanthanum salt and benzotriazole on commercial brass. *Anti Corros. Method. Mater.* **2012**, *59*, 32–38. [CrossRef]
26. Gang, K.; Lingyan, L.; Jintang, L.; Chunshan, C.; Zheng, Z. Study on lanthanum salt conversion coating modified with citric acid on hot dip galvanized steel. *J. Rare Earth* **2010**, *28*, 461–465. [CrossRef]
27. Patil, K.C.; Chandrashekhar, G.V.; George, M.V.; Rao, C.N.R. Infrared spectra and thermal decompositions of metal acetates and dicarboxylates. *Can. J. Chem.* **1968**, *46*, 257–265. [CrossRef]
28. Edwards, D.A.; Hayward, R.N. Transition metal acetates. *Can. J. Chem.* **1968**, *46*, 3443–3446. [CrossRef]
29. García, M.A.; Paje, S.; Llopis, J.; Villegas, M.A. Influencia de las condiciones de preparación en la luminiscencia de recubrimientos de sílice pura. *Bol. Soc. Esp. Ceram. Vidr.* **2000**, *39*, 641–646. (In Spanish) [CrossRef]
30. *ISO-9142 Guía Para la Selección de Condiciones de Envejecimiento Normalizadas de Laboratorio Para Someter a Ensayo Juntas Pegadas*; AENOR: Madrid, Spain, 2004. (In Spanish)
31. *DIN-50018 Sulfur Dioxide Corrosion Testing in a Saturated Atmosphere*; DIN Deutsches Institut für Normung e.V.: Berlin, Germany, 1997.

32. Tétreault, J.; Cano, E.; van Bommel, M.; Scott, D.; Dennis, M.; Barthés-Labrousse, M.G.; Minel, L.; Robbiola, L. Corrosion of copper and lead by formaldehyde, formic acid and acetic acid vapours. *Stud. Conserv.* **2003**, *48*, 237–250. [CrossRef]
33. Krol, D.M.; Smets, B.M.J. Group III ions in sodium silicate glass, 2, Raman study. *Phys. Chem. Glasses* **1984**, *25*, 119–125.
34. Smets, B.M.J.; Krol, D.M. Group III ions in sodium silicate glass, 1, X-ray photoelectron study. *Phys. Chem. Glasses* **1984**, *25*, 113–118.
35. Ellison, A.J.G.; Hess, P.C. Vibrational spectra of high-silica glasses of the system K_2O-SiO_2-La_2O_3. *J. Non Cryst. Solids* **1991**, *127*, 247–258. [CrossRef]
36. Rizzo da Rocha, S.M.; da Silva Queiroz, C.A.; Abrao, A. Synthesis and characterization of lanthanum acetate for application as a catalyst. *J. Alloys Compd.* **2002**, *344*, 389–393. [CrossRef]
37. Bünzli, J.C.G.; Moret, E.; Yersin, J.R. Vibrational spectra of anhydrous lanthanum, europium, gadolinium, and dysprosium nitrates and oxinitrates. *Helv. Chim. Acta* **1978**, *61*, 762–771. [CrossRef]
38. Klingenberg, B.; Vannice, M.A. Influence of pretreatment on lanthanum nitrate, carbonate, and oxide powders. *Chem. Mater.* **1996**, *8*, 2755–2768. [CrossRef]